Supplemental Materials

Molecular Biology of the Cell

Klinke et al.

Online Supplement for Interlocked positive and negative feedback network motifs regulate beta-catenin activity in the adherens junction pathway

David J. Klinke II*†, Nicholas Horvath*, Vanessa Cuppett*,
Yueting Wu*, Wentao Deng*, and Rania Kanj†

*Department of Chemical Engineering and Mary Babb Randolph Cancer Center
†Department of Microbiology, Immunology, and Cell Biology
West Virginia University, Morgantown, WV 25606

June 17, 2015

Contact Info: David J. Klinke II
E-mail: david.klinke@mail.wvu.edu
Phone: (304)293-9346
Fax: (304)293-4139

Department of Chemical Engineering
West Virginia University
P.O. Box 6102
Morgantown, WV 26506-6102

This PDF file includes:

Supplemental Methods

A cue-signal-response model was constructed to represent both prior knowledge about elements of the signaling network and postulated dynamic relationships among the observed molecular species. These causal relationships among the modeled biomolecular species are represented using a mass-action formalism and encoded using a set of ordinary differential equations. Generally, creating a mathematical model of a dynamic system using ordinary differential equations involves two aspects. First, one must assemble the causal relationships thought to underpin the observed phenomena and conservation relationships among related components into a collection of coupled ordinary differential equations. Once the structure (i.e., topology) of the model is specified, one must select values of the model parameters and initial conditions that are consistent with experimental data used to calibrate the model, that is model-based inference. Once calibrated, the model can be used to describe the evolution in the elements of the model as a function of time and to explore the dynamic implications of the assumed model structure. In the following subsections, the model topology and in silico model-based inference of the model parameters will be discussed in more detail.

1. Mathematical model of β-catenin activity in the adherens junction pathway.

As summarized in Figure 7, the cue-signal-response model of the activity of β-catenin in the adherens junction pathway describes the conversion of species within and transport among four different compartments: the nucleus, the cytoplasm, the plasma membrane, and the extracellular space. The particular biochemical species included in the model and a description of their corresponding rate equations are described as follows:

- $[mRw]$: **message RNA for WISP1 in nM**. The rate equation for WISP1 mRNA has two terms. The first term represents a saturable production of WISP1 mRNA that depends on the concentration of multi-protein complexes within the nucleus that contain β-catenin and has a maximum rate of transcription equal to VmW. From a transcription perspective, nuclear β-catenin bound to the cytoplasmic fragment of E-cadherin ($tBEn$) and contained in any other complex (e.g., BEn) are considered equivalent in inducing WISP1 transcription with an affinity equal to KmW. The second term represents the natural decay in WISP1 mRNA, with a rate parameter equal to k_{dm}. We assume that the rate parameter for mRNA degradation is the same for all mRNAs included in the model.

$$\frac{d[mRw]}{dt} = \frac{VmW \cdot tBEn}{KmW + tBEn} - k_{dm} \cdot mRw \tag{1}$$

- $[mRb]$: **message RNA for β-catenin in nM**. Similar to the rate equation for $[mRw]$, the first term represents a saturable production of β-catenin mRNA that depends on the concentration of multi-protein complexes within the nucleus that contain β-catenin and has a maximum rate of transcription equal to VmB. The affinity of nuclear complexes that contain β-catenin for the promoter region is equal to KmB. Similarly, the decay in β-catenin mRNA is represented by the second term with the rate parameter in common with $[mRw]$, kdm.

$$\frac{d[mRb]}{dt} = \frac{VmB \cdot tBEn}{KmB + tBEn} - k_{dm} \cdot mRb \tag{2}$$

- $[mRe]$: **message RNA for E-cadherin in nM**. E-cadherin mRNA was assumed to have a saturable production that depends on the concentration of multi-protein complexes within

the nucleus that contain β-catenin and to have a maximum rate of transcription equal to RmE. The affinity of nuclear complexes that contain β-catenin for the E-cadherin promoter region is equal to KmE. Degradation of message for E-cadherin is represented by the second term.

$$\frac{d[mRe]}{dt} = \frac{VmE \cdot tBEn}{KmE + tBEn} - k_{dm} \cdot mRe. \tag{3}$$

- $[Wc]$: **WISP1 protein in cytosol in nM**. The rate of change in cytoplasmic WISP1 depends on the balance between protein translation from WISP1 mRNA and the extracellular release of WISP1 with a rate parameter equal to k_s. We assume that the rate constant for protein translation from mRNA (k_p) is the same for all proteins.

$$\frac{d[Wc]}{dt} = k_p \cdot mRw - k_s \cdot Wc \tag{4}$$

- $[We]$: **secreted WISP1 present in cell-conditioned media in nM**. WISP1 accumulates in the cell-conditioned media with a rate equal to the product of the rate of cellular WISP1 secretion, the total number of cells (Ct), and the ratio of x volume (Vc) to media volume (Vt). The cytosolic volume is estimated from a diameter of 20 μm of a B16F0 cell and a nuclear compartment of 1/7 of the size of the cytoplasm.

$$\frac{d[We]}{dt} = k_s \cdot Wc \cdot Ct \cdot \frac{V_c}{V_t} \tag{5}$$

- $[Bc]$: **free β-catenin present in cytosol in nM**. The rate of change in free β-catenin depends on the sum of three terms: protein translation from β-catenin mRNA, binding of free β-catenin with free E-cadherin to form a complex associated with endosomes in the cytoplasm, and dissociation of this cytoplasmic E-cadherin/β-catenin complex. As the model focuses on the adherens junction pathway, we assume that β-catenin binds only to E-cadherin and that the copy numbers of β-catenin sequestered as part of the canonical Wnt pathway is negligible.

$$\frac{d[Bc]}{dt} = k_p \cdot mRb - k_{f1} \cdot Bc \cdot Ec + k_{r1} \cdot BEc \tag{6}$$

- $[Ec]$: **free E-cadherin present in cytosol in nM**. The rate of change in free E-cadherin depends on the sum of four terms: protein translation from E-cadherin mRNA, binding of free β-catenin with free E-cadherin to form an endosomal-related complex in the cytosol, dissociation of this cytoplasmic E-cadherin/β-catenin complex, and proteasomal degradation of free E-cadherin in the cytosol. The rate of proteasomal degradation is saturable, where complexes containing E-cadherin compete for degradation with a half-max concentration equal to KmP and maximum rate equal to VmP.

$$\begin{aligned} \frac{d[Ec]}{dt} &= k_p \cdot mRe - k_{f1} \cdot Bc \cdot Ec + k_{r1} \cdot BEc - ... \\ &\quad \frac{VmP \cdot Ec}{KmP + tBEc + Ec} \end{aligned} \tag{7}$$

- $[BEc]$: **Multi-protein complex containing E-cadherin and β-catenin present in cytosol in nM**. The first two terms describe the net rate of complex formation from free E-cadherin and free β-catenin. The net rate of transport to the cell membrane by the balance

between exocytosis versus endocytosis are represented by the third and fourth terms. The ratio of volumes accounts for the change in concentration due to differences in compartment size. The volume of the membrane compartment (V_m) was estimated based on a spherical cell diameter of 20 μm and a membrane thickness of 10 nm (BioNumbers ID 100787 [1]). This multi-protein complex can also be transferred to lysosomes where it can be degraded [2], which is captured by the fifth term. The model also included an alternative hypothesis regarding the fate of endocytosed multi-protein complex containing E-cadherin and β-catenin. Lysosomes also contain pH-activated proteases, including the cysteine protease cathepsin B. E-cadherin is a substrate of cathepsin B suggesting that lysosomal degradation may also involve liberating the cytoplasmic portion of the multi-protein complex containing E-cadherin and β-catenin, which is represented by the sixth term. This proteolytic reaction creates the positive feedback control motif. This cleaved multi-protein complex then joins the cytoplasmic pool of truncated E-cadherin/β-catenin complex where it can be degraded by the proteasome, which creates the negative feedback control motif. The presence of other proteins of the adherens junction complex, namely alpha-catenin and p120-catenin, are implicitly assumed [3].

$$\begin{aligned}\frac{d[BEc]}{dt} &= k_{f1}\cdot Bc\cdot Ec - k_{r1}\cdot BEc - k_{f2}\cdot BEc + ... \\ & \quad k_{r2}\cdot BEm\cdot\frac{V_m}{V_c} - k_{ld}\cdot BEc - k_l\cdot BEc \end{aligned} \tag{8}$$

- $[BEm]$: **Multi-protein complex containing E-cadherin and β-catenin present in cell membrane in nM**. The net transport of the adherens junction protein complex containing E-cadherin and β-catenin to the membrane depends on the balance in rates of exocytosis and endocytosis, the first two terms. Enzymatic cleavage of the extracellular portion of E-cadherin to create a new molecular protein complex is represented by the third term, where the enzymatic cleavage rate constant is a function of time in hours ($k_e(t)$), as shown in Equation 10. The last two terms describe the sequestration at the cell membrane of the proteins contained within the adherens junction protein complex whereby cadherin repeats form extracellular bonds, which facilitates cell adhesion. We assume that the total number of extracellular binding sites to which a cell can adhere is fixed ($Esites$) and cadherin repeats contained within the adherens junction protein complex compete for these binding sites. This implies that the effective concentration of free extracellular binding sites can be replaced by the algebraic constraint (i.e., $Esites_{free} = Esites - BEmb$).

$$\begin{aligned}\frac{d[BEm]}{dt} &= k_{f2}\cdot BEc\cdot\frac{V_c}{V_m} - k_{r2}\cdot BEm - k_e(t)\cdot BEm - ... \\ & \quad k_{f4}\cdot BEm\cdot(Esites - BEmb) + k_{r4}\cdot BEmb \end{aligned} \tag{9}$$

$$k_e(t) = 3\cdot(erf[100\cdot(t-0.1)] - erf[100\cdot(t-0.8)]) \tag{10}$$

- $[BEmb]$: **Multi-protein complex containing E-cadherin and β-catenin bound to extracellular E-cadherin binding site in nM**. This species represents the concentration of adherens junction protein complexes sequestered at the cell membrane through extracellular binding to cell adhesion sites. The first two terms represent the dynamics of this competition for extracellular binding sites. Irreversible enzymatic conversion of the adherens junction protein complexes to contain the cytoplasmic fragment instead of the full length E-cadherin is represented by the third term, where the enzymatic cleavage rate constant is a function of time ($k_e(t)$).

$$\frac{d[BEmb]}{dt} = k_{f4}\cdot BEm\cdot(Esites - BEmb) - k_{r4}\cdot BEmb - k_e(t)\cdot BEmb \tag{11}$$

- $[tBEm]$: **Multi-protein complex containing the cytoplasmic fragment of E-cadherin and β-catenin present in cell membrane in nM**. This species is formed upon enzymatic cleavage of the extracellular portion of E-cadherin from the adherens junction protein complex, which is represented by the first two terms. The net rate of transport away from the cell membrane of this truncated protein complex depends on the balance between endocytosis and exocytosis, as represented by the last two terms. The last term is multiplied by a volume ratio to account for concentration changes due to differences in volumes between the membrane and cytoplasm compartments.

$$\frac{d[tBEm]}{dt} = k_e(t) \cdot BEmb + k_e(t) \cdot BEm - k_{r5} \cdot tBEm + k_{f5} \cdot tBEc \cdot \frac{V_c}{V_m} \tag{12}$$

- $[tBEc]$: **Multi-protein complex containing the cytoplasmic fragment of E-cadherin and β-catenin present in cytosol in nM**. The cytosolic concentration of the protein complex containing the cytoplasmic fragment of E-cadherin and β-catenin depends on the net rate of transport from the cell membrane, as represented by the first two terms; the rate of formation from the lysosomal cleavage of BEc; the net rate of transport to the nucleus, as represented by the fourth and fifth terms; and the rate of proteasomal degradation, as represented by the last term. The rate of proteasomal degradation is saturable where all cytoplasmic species that contain E-cadherin compete for degradation.

$$\begin{aligned} \frac{d[tBEc]}{dt} &= k_{r5} \cdot tBEm \cdot \frac{V_m}{V_c} - k_{f5} \cdot tBEc + k_l \cdot BEc - k_{f3} \cdot tBEc + ... \\ & \quad k_{r3} \cdot tBEn \cdot \frac{V_n}{V_c} - \frac{VmP \cdot tBEc}{KmP + tBEc + Ec} \end{aligned} \tag{13}$$

- $[tBEn]$: **Multi-protein complex containing the cytoplasmic fragment of E-cadherin and β-catenin present in nucleus in nM**. The dynamics of nuclear protein complexes that contain β-catenin and the cytoplasmic fragment of E-cadherin depend on the balance between nuclear import and export, as represented by these two respective terms. The first term is multiplied by a volume ratio to account for concentration changes due to to differences in compartment volumes.

$$\frac{d[tBEn]}{dt} = k_{f3} \cdot tBEc \cdot \frac{V_c}{V_n} - k_{r3} \cdot tBEn \tag{14}$$

The model equations were encoded and evaluated in MatLab R2013a (The MathWorks, Natick, MA). As the experimental measurements do not directly correspond to individual molecular species in the mathematical model, the simulated concentrations of the species in the model were combined to represent the experimental measurements. The values for total cellular β-catenin (β-cat$_{Tot}$) and E-cadherin (E-cad$_{Tot}$) were represented as the sum over all species that contain the corresponding proteins times the compartmental volumes, as shown by:

$$\begin{aligned} \beta\text{-cat}_{Tot} &= V_c \cdot (Bc + BEc + tBEc) + V_m \cdot (BEm + BEmb + tBEm) + ... \\ & \quad V_n \cdot tBEn \end{aligned} \tag{15}$$

and

$$\begin{aligned} \text{E-cad}_{Tot} &= 0.6 \cdot (V_c \cdot (Ec + BEc + tBEc) + V_m \cdot (BEm + BEmb + tBEm) + ... \\ & \quad V_n \cdot tBEn. \end{aligned} \tag{16}$$

In Equation 16, the sum of the species containing E-cadherin are multiplied by a factor of 0.6. This coefficient represents that fact that, while the mathematical model just includes E-cadherin, B16F0 cells may express other cadherins in lower abundance than E-cadherin that also form multi-protein complexes with β-catenin and that have analogous biological function. Similarly, the ratios of β-catenin and E-cadherin in the nucleus to cytoplasm were calculated based on the sum of species in a particular compartment multiplied by the compartmental volume, as follows:

$$\beta\text{-cat}_{N/C} = \frac{V_n \cdot (tBEn + Bg)}{V_c \cdot (Bc + BEc + tBEc + Bg) + V_m \cdot (BEm + BEmb + tBEm + Bg)} \tag{17}$$

and

$$\text{E-cad}_{N/C} = \frac{V_n \cdot (tBEn + Bg)}{V_c \cdot (Ec + BEc + tBEc + Bg) + V_m \cdot (BEm + BEmb + tBEm + Bg)}. \tag{18}$$

As background fluorescence limits the ability to quantify changes in abundance between the different compartments, an additional term (Bg) was added to represent this background fluorescence and set equal to 3.16.

As the initial values for many of the biomolecular species are unknown and that the values of the parameters also influence these initial values, the system was simulated using multiple trypsinization cycles, with a single cycle having a 25 hour duration. The third trypsinization cycle was used to compare against the observed data. Summed squared error between experimental and simulated measurements was used to determine goodness-of-fit. The model parameters are listed in Table S1. The parameters listed in Table S2 were allowed to vary in simulating the iCRT14 experiments, while the remaining parameters were kept the same between the two experimental conditions. Maximum expectation estimates for the calibrated parameters, shown in Tables S1 and S2, were determined using an empirical Bayesian approach [4], as described in the next section.

2. In silico model-based inference of model predictions and parameters

An empirical Bayesian approach was used to estimate the uncertainty associated with the model predictions and parameters, given the available experimental data [4]. Briefly, we used an Adaptive Markov Chain Monte Carlo (AMCMC) algorithm to generate a sequence of states that represent samples drawn from the posterior distribution of the model predictions, given the uncertainty in the model parameters and the specific calibration data. A starting point in the parameter space was obtained via simulated annealing [5]. To accelerate the equilibration of the model behavior, final values were captured after the simulated annealing step and used as initial values for the in silico model-based inference simulations. Using an unbiased prior distribution, a learning period of 100,000 steps was used to establish the covariance of the proposal distribution. The proposed steps within parameter space were evaluated using a Metropolis-Hastings algorithm with a targeted acceptance fraction equal to 0.2. The Gelman-Rubin potential scale reduction factor was applied to the model predictions to estimate the convergence of the Markov chain to the posterior distribution of the model predictions [6, 7]. The posterior distribution in the model predictions and model parameters were estimated from the converged segments of the Markov chains. In addition, representative samples from the posterior distribution were obtained by retaining every 200th step of the cumulative Markov chain.

Four parallel chains, each containing at least 5×10^5 steps, were calibrated to the observed experimental data (see Figure 8 in main text) and used to estimate the posterior distributions in the model predictions and parameters. The simulation of each chain took approximately 720 hours on a single core of a 2.66 GHz Dual-Core Intel Xeon 64-bit processor with 8 GB RAM.

A graphical summary of the Gelman-Rubin statistics was used to as a diagnostic to determine convergence of the Markov chains to the posterior distribution in the model predictions (Figure S4). An initial sequence of 3×10^5 AMCMC steps was required for the four chains to converge. This initial sequence was used as the "burn-in" period. Traces for each of the parameters were used to estimate the degree of mixing among the four chains (see Figure S5). The optimal parameter values were determined using the expectation maximum and are listed in Table S1. Pairwise scatter plots obtained from the four chains following the burn-in period were used to estimate the posterior identifiability of the model parameters (see Figure S6). The scatter plots were colored based upon marginal posterior probability density obtained by kernel density estimation. A high value for the correlation coefficient suggests that the parameters were not independently identifiable given the calibration data. For example, the parameters associated with the maximum rate for E-cadherin gene translation (e.g., VmE) and the maximum rate of β-catenin gene translation (e.g., VmB) were not identifiable, as they exhibited a correlation coefficient of 1.0. The posterior distributions in the model predictions were obtained by marginalizing the model predictions over all of the parameter values from the Markov chains following the burn-in period. Despite the variation in the cue-signal-response model parameters, the posterior predictions obtained from the converged segment of the Markov chains resulted in a narrow range of predictions (see Figure 8 in main text).

References

[1] Moran, U., Phillips, R. & Milo, R. SnapShot: key numbers in biology. *Cell* **141**, 1262–1262 (2010).

[2] Yap, A. S., Crampton, M. S. & Hardin, J. Making and breaking contacts: the cellular biology of cadherin regulation. *Curr. Opin. Cell Biol.* **19**, 508–514 (2007).

[3] Yamada, S., Pokutta, S., Drees, F., Weis, W. I. & Nelson, W. J. Deconstructing the cadherin-catenin-actin complex. *Cell* **123**, 889–901 (2005).

[4] Klinke, D. J. An empirical bayesian approach for model-based inference of cellular signaling networks. *BMC Bioinform* **10**, 371 (2009).

[5] Beers, K. J. *Numerical methods for chemical engineering. Applications in Matlab* (Cambridge university Press, Cambridge, 2007).

[6] Gelman, A. & Rubin, D. Inference form iterative simulation using multiple sequences. *Statistical Science* **7**, 457–474 (1992).

[7] Brooks, S. & Gelman, A. General methods for monitoring convergence of iterative simulations. *Journal of Computational and Graphical Statistics* **7**, 434–455 (1998).

[8] Kholodenko, B. N., Demin, O. V., Moehren, G. & Hoek, J. B. Quantification of short term signaling by the epidermal growth factor receptor. *J Biol Chem* **274**, 30169–30181 (1999).

[9] Alberts, B. *et al. Molecular biology of the cell* (Garland Publishing, New York, 2002).

[10] Ivascu, A. & Kubbies, M. Diversity of cell-mediated adhesions in breast cancer spheroids. *Int. J. Oncol.* **31**, 1403–1413 (2007).

Table S1: **List of cue-signal-response model parameters and corresponding values.**

Symbol	Definition	Value	Units	Refs
k_{dm}	Degradation of mRNA	2.81×10^{5}	hr^{-1}	–
$k_e(t)$	Enzymatic cleavage of extracellular portion of E-cadherin	Eqn. 10	hr^{-1}	–
k_{ld}	Complete lysosomal degradation of adherens junction protein complexes	9.10×10^{-3}	hr^{-1}	–
k_l	Lysosomal cleavage that creates truncated adherens junction protein complexes	1.95×10^{-1}	hr^{-1}	–
k_p	Protein translation from mRNA	5.40×10^{-1}	hr^{-1}	–
k_s	Extracellular release of WISP1 protein	4.02×10^{1}	hr^{-1}	–
k_{f1}	Association of cytoplasmic β-catenin with E-cadherin	1.11×10^{3}	$nM \cdot hr^{-1}$	–
k_{r1}	Dissociation of cytoplasmic β-catenin-E-cadherin complex	5.70×10^{-3}	hr^{-1}	–
k_{f2}	Exocytosis of intact adherens junction protein complexes	1.45×10^{5}	hr^{-1}	–
k_{r2}	Endocytosis of intact adherens junction protein complexes	5.58×10^{6}	hr^{-1}	–
k_{f3}	Nuclear import of cytoplasmic β-catenin-containing complex	8.50×10^{4}	hr^{-1}	–
k_{r3}	Nuclear export of cytoplasmic β-catenin-containing complex	3.06×10^{1}	hr^{-1}	–
k_{f4}	Association of adherens junction protein complex with extracellular binding site	1.52×10^{2}	$nM \cdot hr^{-1}$	–
k_{r4}	Dissociation of adherens junction protein complex with extracellular binding site	7.79×10^{-3}	hr^{-1}	–
k_{f5}	Exocytosis of truncated adherens junction protein complexes	5.19×10^{1}	hr^{-1}	–
k_{r5}	Endocytosis of truncated adherens junction protein complexes	9.42×10^{-1}	hr^{-1}	–
VmP	Maximum proteasomal degradation rate of protein complexes	3.42×10^{1}	$nM \cdot hr^{-1}$	–
KmP	Half-maximal constant for protein complex binding to proteasome	2.55×10^{-3}	nM	–
VmW	Maximum synthesis rate of WISP1 mRNA	5.89×10^{4}	$nM \cdot hr^{-1}$	–
KmW	Half-maximal constant for β-catenin complex binding to *Wisp1* promoter	9.93×10^{-5}	nM	–
VmB	Maximum synthesis rate of β-catenin mRNA	3.72×10^{6}	$nM \cdot hr^{-1}$	–
KmB	Half-maximal constant for β-catenin complex binding to *Ctnnb1* promoter	5.24×10^{-2}	nM	–
VmE	Maximum synthesis rate of E-cadherin mRNA	1.67×10^{7}	$nM \cdot hr^{-1}$	–
KmE	Half-maximal constant for β-catenin complex inducing *Cdh1* expression	1.76×10^{-1}	nM	–
$Esites$	Number of extracellular binding sites for E-cadherin	4.72×10^{3}	nM	–
Ct	Number of cells per well in a 96-well plate	6.0×10^{4}	$cells$	–
V_t	Volume of well in a 96-well plate	1.5×10^{-4}	L	–
V_c	Equivalent volume of cytoplasm compartment	3.67×10^{-12}	L	[8]
V_m	Equivalent volume of membrane compartment	1.26×10^{-14}	L	[8]
Vc/Vn	Ratio of cytoplasm volume relative to nucleus	7	–	[9]

The values for the reaction rate parameters correspond to the maximum expectation values.

Table S2: **Values of model parameters that are altered due to the presence of the Wnt-pathway inhibitor, iCRT14.**

Symbol	Definition	Value	Units	Refs
k_{f3}	Rate constant for nuclear import of cytoplasmic β-catenin-containing complex in presence of 25 μM iCRT14	2.22×10^{-7}	hr^{-1}	–
k_{r3}	Rate constant for nuclear export of cytoplasmic β-catenin-containing complex in presence of 25 μM iCRT14	7.05×10^{-2}	hr^{-1}	–
KmW	Half-maximal constant for β-catenin complex binding to *Wisp1* promoter with 25 μMiCRT14	1.11×10^{2}	nM	–
KmB	Half-maximal constant for β-catenin complex binding to *Ctnnb1* promoter with 25 μMiCRT14	1.30×10^{4}	nM	–
KmE	Half-maximal constant for β-catenin complex binding to *Cdh1* promoter with 25 μMiCRT14	1.01×10^{-5}	nM	–

The values for the reaction rate parameters correspond to the maximum expectation values.

Table S3: **Evaluation of different cell lines as appropriate cell models to validate network model of β-catenin activity in the adherens junction pathway.** Cells were cultured in tissue culture plates at a similar density. After 24 hours, WISP1 was assayed in media conditioned by the indicated cell lines and WISP1 mRNA was assayed in cell lysates.

Cell line	Description	Tight spheroid formation	Spheroid depends on E-cadherin	WISP1 qRT-PCR		WISP1 ELISA[1]
				Present	ΔCt GAPDH (cycles)	24hr CDM (pg/ml)
B16F0	Mm malignant melanocyte	Yes	Yes	Yes	8.9 ± 0.3	500
B16F10	Mm malignant melanocyte	Yes	Yes	Yes	6.5 ± 0.2	>1000
Melan-A	Mm normal melanocyte	Yes	Yes	Yes	4.0	500-1000
Hs578T	Hs Claudin low Br Ca	Yes	Yes	Yes	4.0 ± 1.0	700
BT474	Hs HER2+ Br Ca	Yes	Yes	ND	> 21	ND
MCF7	Hs Luminal A Br Ca	–	–	ND	> 21	ND
T47D	Hs Luminal B Br Ca	–	–	ND	> 21	ND

Br Ca: breast carcinoma, CDM: cell-conditioned media, ND: not detected, – : not tested, Hs: human cell line, Mm: mouse cell line. Results for qRT-PCR are shown as mean ± s.d.

[1] WISP1 was also assayed by ELISA in cell culture media prior to cell-conditioning and was not detected.

Table S4: **List of PCR primers.**

Gene	Forward Sequence (5' to 3')	Reverse Sequence (5' to 3')
h/mGapdh	TGCACCACCAACTGCTTAGC	GGCATGGACTGTGGTCATGAG
HsWISP1	AGAGCCGCCTCTGCAACTT	GGAGAAGCCAAGCCCATCA
MmWisp1	CGTGGAGCAACGGTATGAG	GAGAGTGAAGTTCGTGGCC
HsCCND1	TATTGCGCTGCTACCGTTGA	CCAATAGCAGCAAACAATGTGAAA
MmCcnd1	GTTCATTTCCAACCCACCCTC	AGAAAGTGCGTTGTGCGGTAG
MmCdh1	CAGCCTTCTTTTCGGAAGACT	GGTAGACAGCTCCCTATGACTG
MmCtnnb1	TCTTCAGGACAGAGCCAATGG	ACCAGAGTGAAAAGAACGGTAGCT

Supplemental Figures

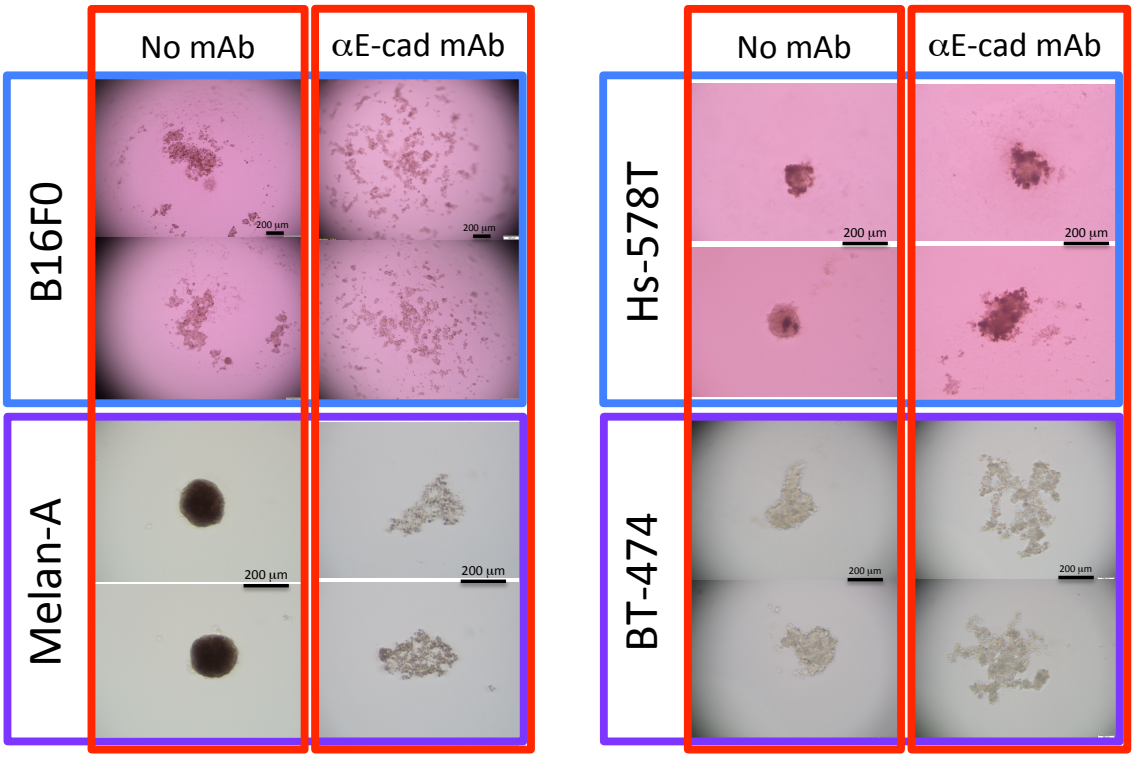

Figure S1: **The effect of a neutralizing E-cadherin antibody (DECMA-1) on spheroid formation.** Hanging drop cultures of B16F0, Melan-A, Hs-578T, and BT-474 cells were established at a cell density of 10,000 cells per ml in tissue culture media alone or with tissue culture media supplemented with 50 μg/ml of a neutralizing rat monoclonal IgG1 against E-cadherin (DECMA-1). Cells were imaged after 3 days. BT-474 have been previously reported to form tight spheroids that are dependent on homotypic E-cadherin binding [10].

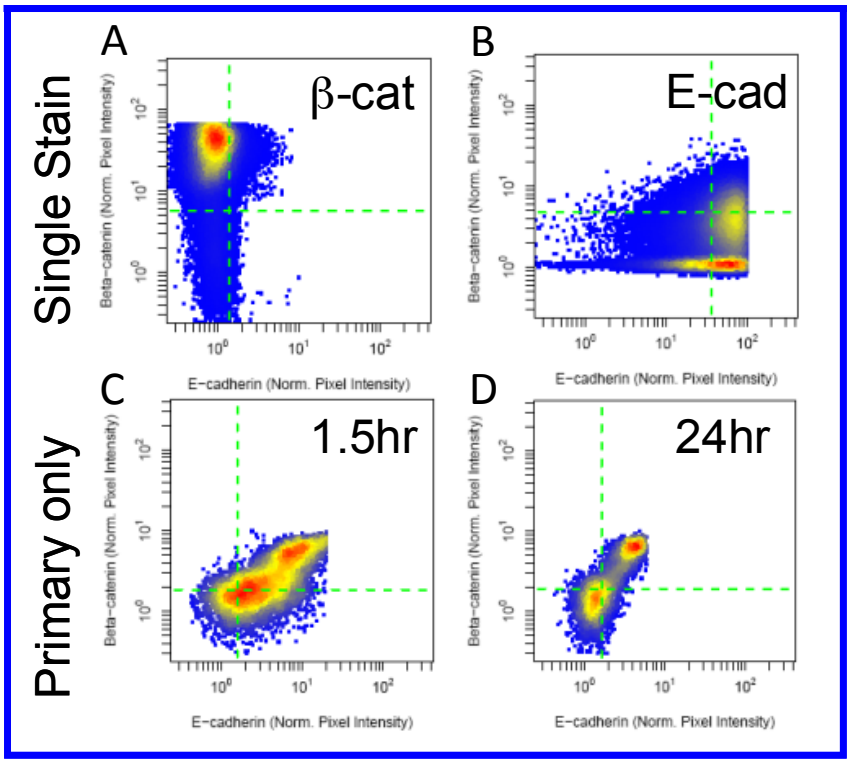

Figure S2: **Confocal fluorescence microscopy of Beta-catenin and the cytoplasmic fragment of E-cadherin using fluorophore-conjugated primary antibodies.** Cells were single stained with fluorophore-conjugated primary antibodies against beta-catenin (A) and E-cadherin (B). Following trypsinization, cells were stained with fluorophore-conjugated antibodies against both beta-catenin and E-cadherin (1.5 hours: C and 24 hours: D). Fluorescence intensity associated with AlexaFluor488 (beta-catenin) and AlexaFluor647 (E-cadherin) channels for each pixel within the confocal image are shown as scatter plots. As would be expected for sequential scanning of the fluorescent channels, the results for singly stained cells exhibit negligible fluorescent spillover into the opposite fluorescent channel (A and B). In cells stained with both fluorophore-conjugated primary antibodies, pixels are either double negative or double positive for beta-catenin and E-cadherin staining at both 1.5 and 24 hours following disruption of adherens junctions (C and D). Collectively, the results suggest that co-localization of beta-catenin and E-cadherin observed in confocal fluorescence microscopy is not a staining artifact introduced by cross-reactivity of the secondary antibodies.

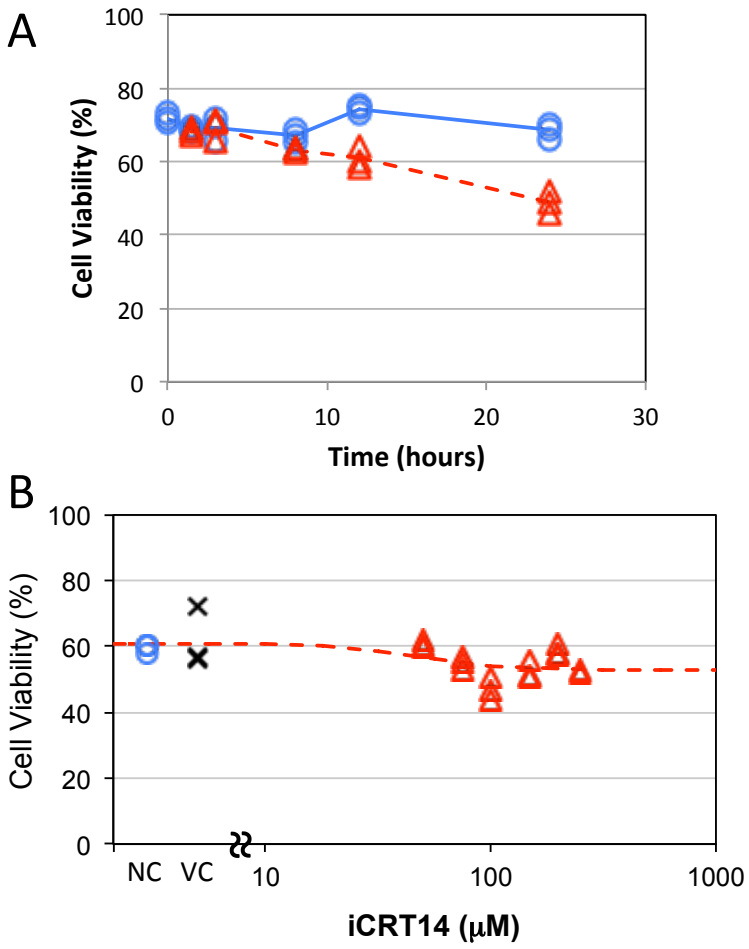

Figure S3: **The effect of iCRT14 on cell viability.** In addition to quantifying live cell density, cell viability was also assayed simultaneously under the experimental conditions shown in panels E and F of Figure 9. Specifically, the cell viability of B16F0 cells was assessed by flow cytometry in two ways. (A) First, cell viability was assayed as a function of time following trypsinization when cultured in sDMEM (blue circles) and in sDMEM with 25μM iCRT14 (red triangles). The corresponding cell densities are shown in Figure 9E. (B) Second, cell viability was assayed at 24 hours when cultured in sDMEM (blue circles - negative control (NC)), sDMEM plus DMSO (x - vehicle control (VC)), and sDMEM plus increasing concentrations of iCRT14 (red triangles). The corresponding cell densities are shown in Figure 9F.

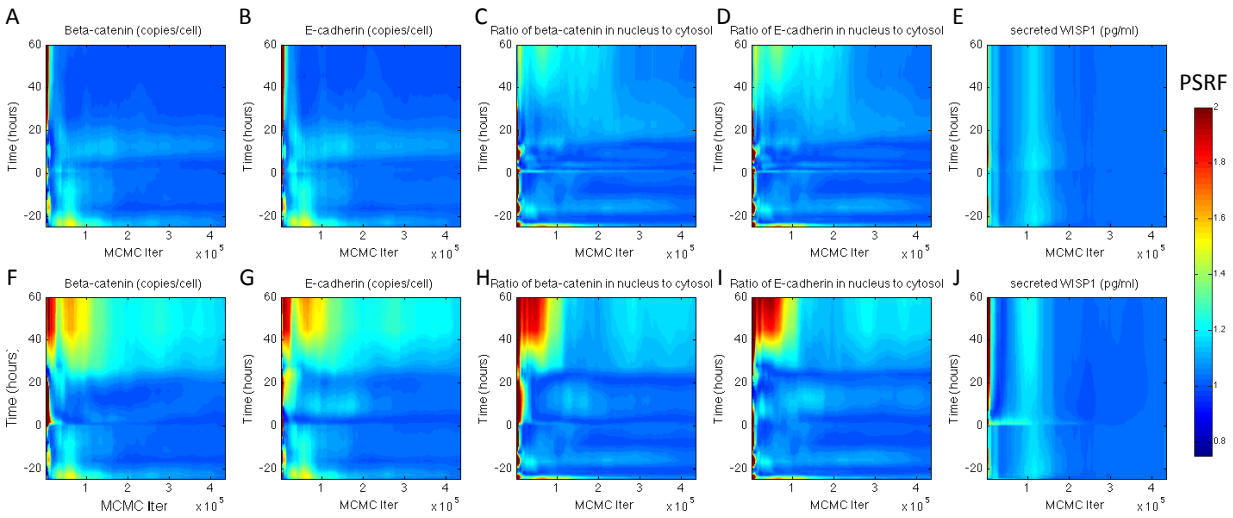

Figure S4: **Convergence of AMCMC results for the cue-signal-response model.** A contour plot of the Gelman-Rubin potential scale reduction factor (PSRF) statistic of the model predictions shown as functions of time (i.e., the y-axis) and AMCMC step (i.e., the x-axis). Four parallel chains were used to calculate the Gelman-Rubin statistics for the model-based inference of the observed cellular response following trypsinization alone (A-E) and iCRT14 plus trypsinization (G-L). The modeled cellular responses include total cellular β-catenin (A,F), total cellular E-cadherin (B,G), ratio of β-catenin in nucleus versus cytoplasm, ratio of E-cadherin in nucleus versus cytoplasm, and secreted WISP1. Values of the PSRF less than 1.2 suggest convergence of the chains.

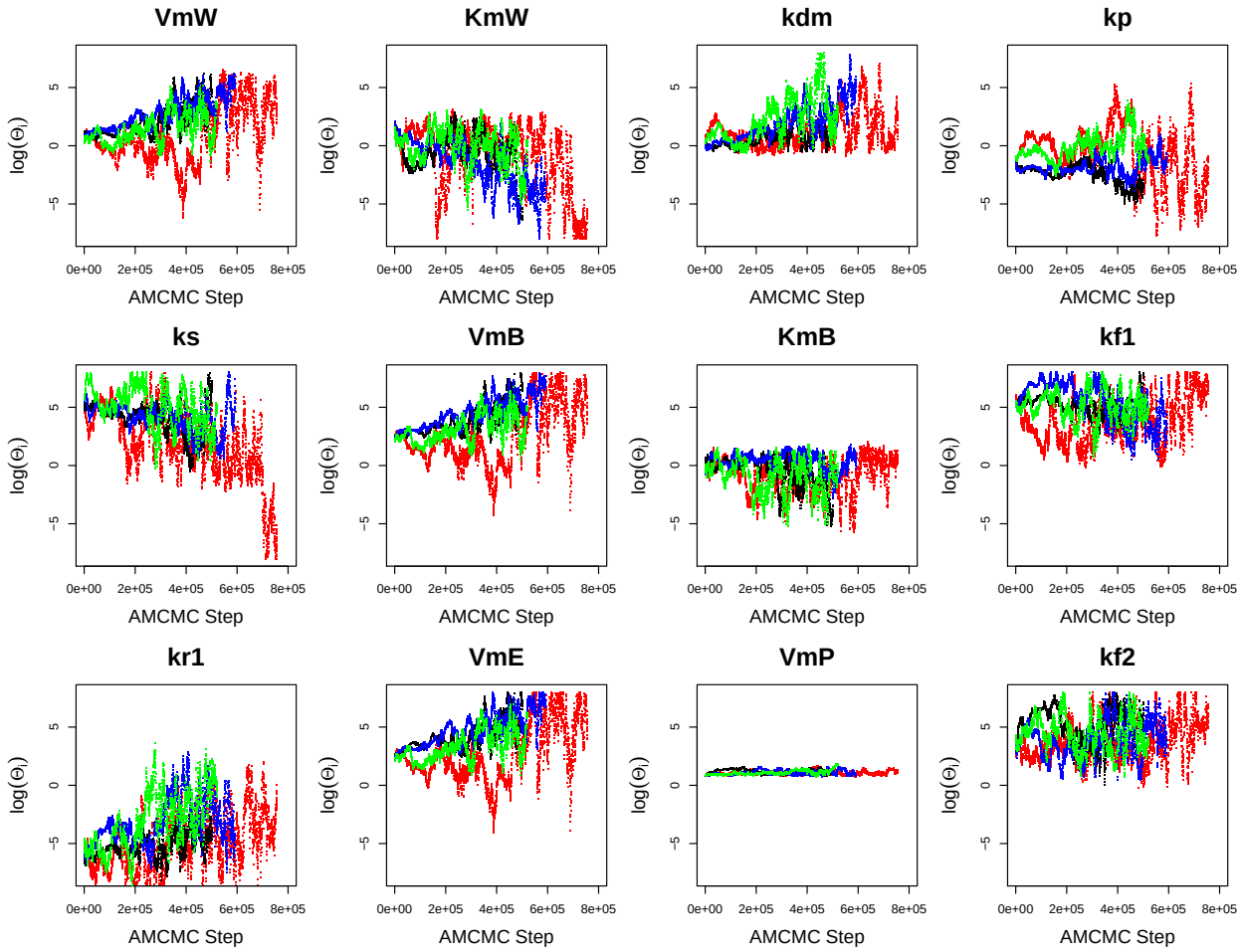

Figure S5: **AMCMC summary plots for each of the model parameters.** The trace of each of the model parameters is shown as a function of AMCMC step, where the parameter name is indicated above the panel. The traces for four parallel chains are shown in different colors: chain 1 (blue), chain 2 (black), chain 3 (red), and chain 4 (green). The last panel is the trace of the posterior likelihood ($P(Y|M,\theta)$) for each of the AMCMC chains.

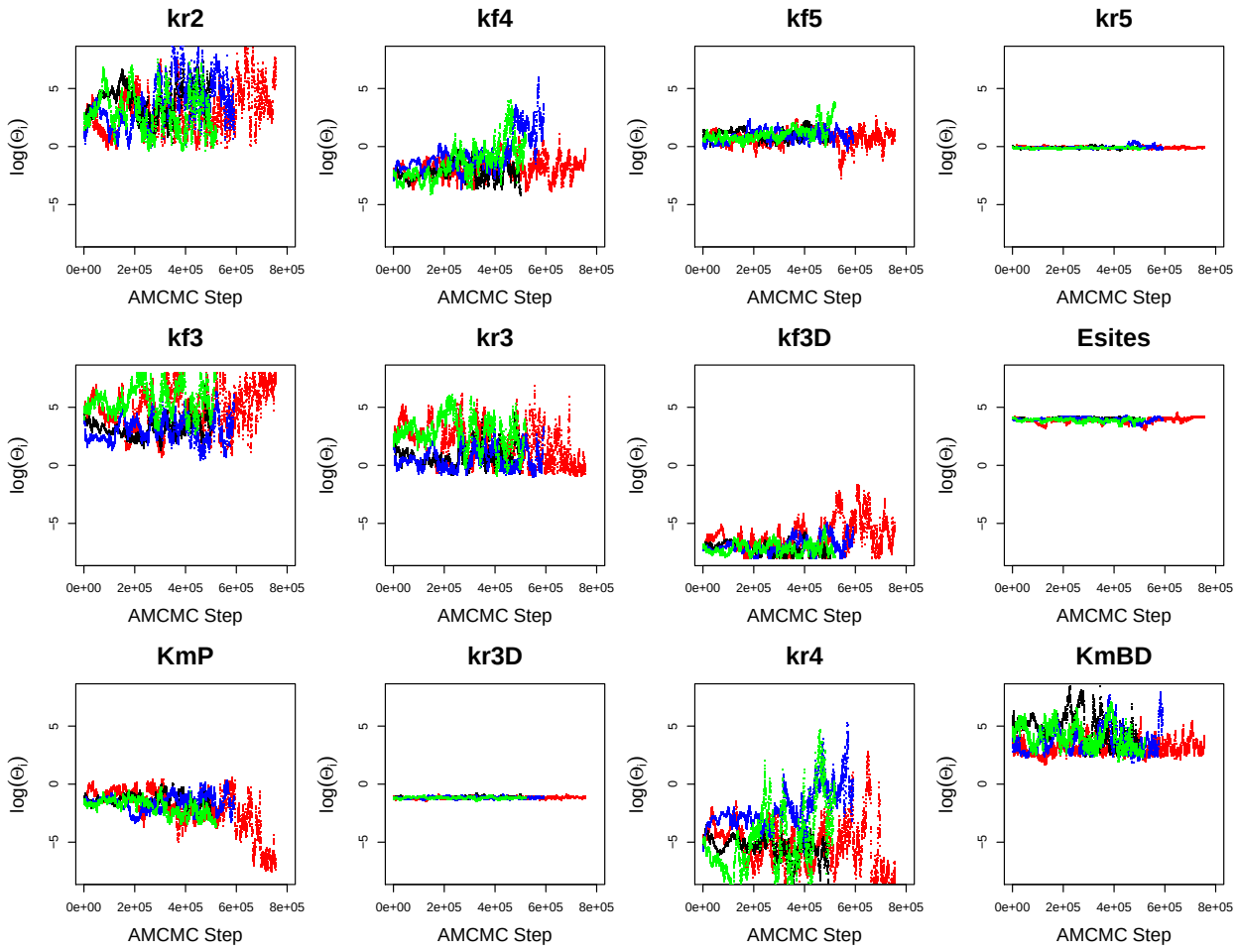

Figure S5 - continued.

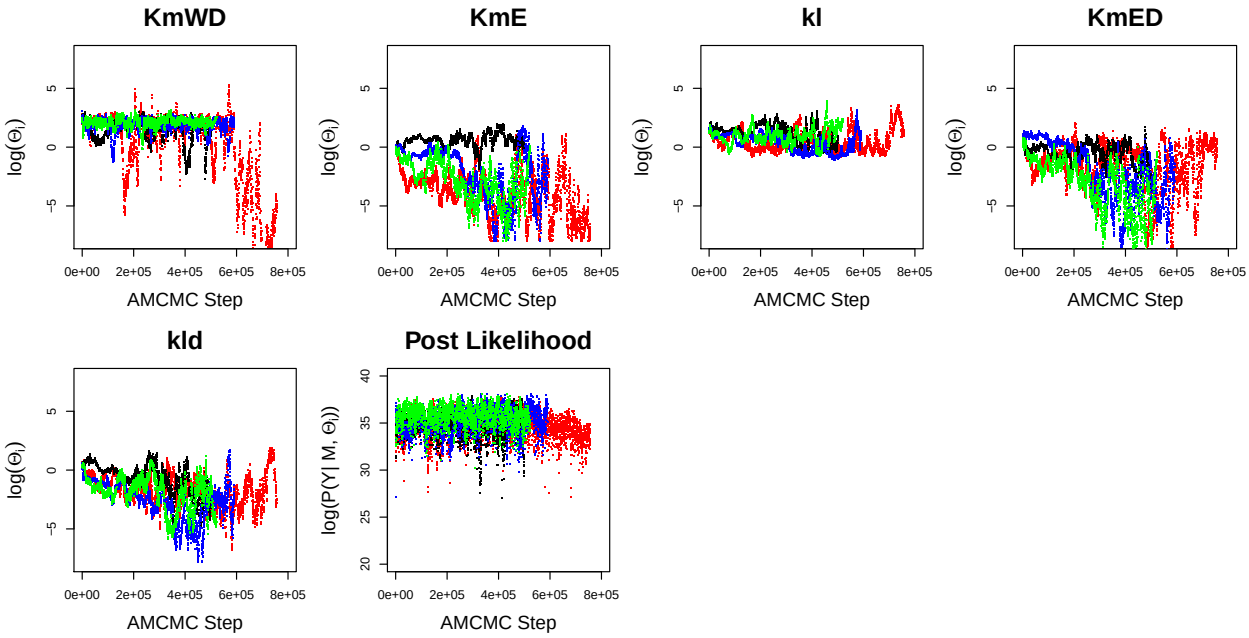

Figure S5 - continued.

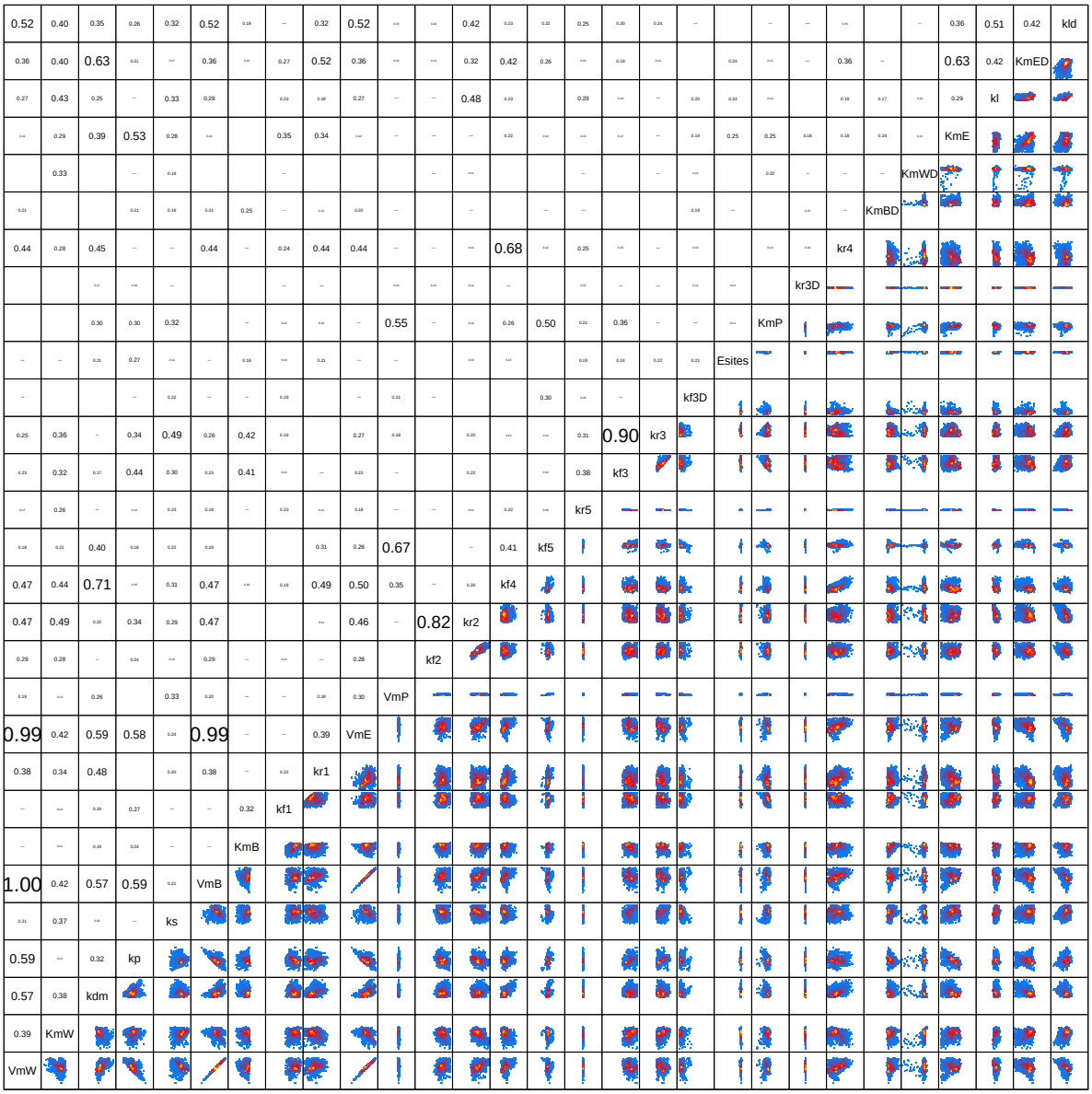

Figure S6: **Pairwise comparison of posterior distribution in cue-signal-response rate parameters.** Parameter names are given on the diagonal. Above the diagonal are the pairwise correlation coefficients of the parameters obtained from the four thinned Markov chains. Pairwise projections of the marginalized probability density in $\log_{10}$ space are given below the diagonal. Coloring is based upon the estimated 2-D posterior density distributions using kernel density estimation. The axes for the scatter plots each spans from 10^{-8} to 10^{8}.

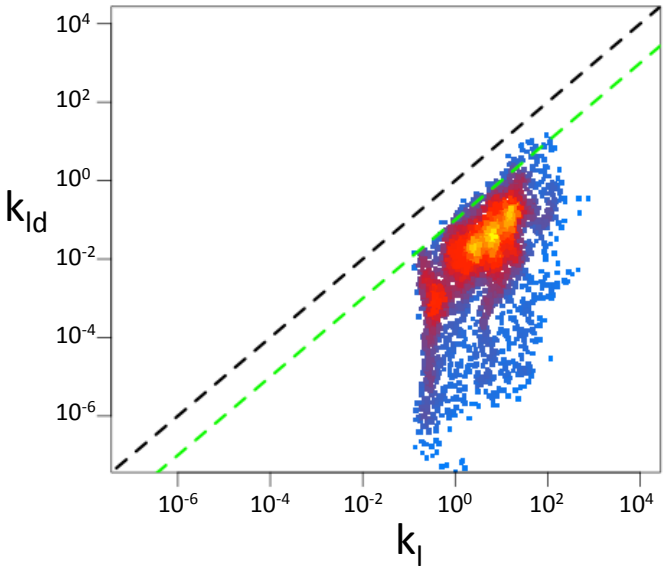

Figure S7: **Scatter plot of the posterior distribution in parameters associated with the fate of endocytosed multi-protein complex containing beta-catenin and E-cadherin.** The endocytosed complex, BEc, is degraded by a total degradation pathway, which corresponds to the rate parameter k_{ld}, and a partial degradation pathway, which corresponds to the rate parameter k_l, that results in the release of beta-catenin to the cytosolic pool. Values of k_{ld} and k_l that are equal lie along the diagonal (dotted black line) and values of k_{ld} that are a factor of 10 or more below the values of k_l lie below the dotted green line. Coloring is based upon the estimated 2-D posterior density distributions using kernel density estimation.

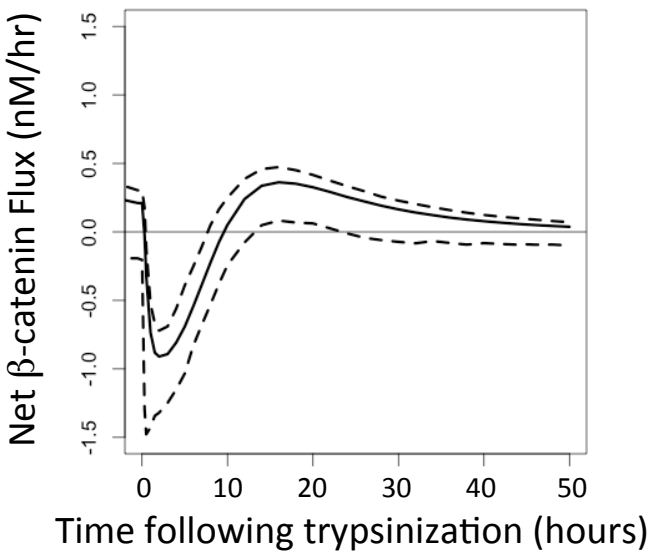

Figure S8: **Posterior distribution in the net rate of change in beta-catenin, expressed in terms of nM per hour, as a function of time following trypsinization.** The most likely predictions are represented by the solid line and the dashed lines enclose the 90% confidence interval.